Reply to Reviewer 2

The article presents a novel approach to inferring ozone formation sensitivity on a global scale. The authors combine two widely used indicators—the ozone weekend effect (WE-WD O_3) and the formaldehyde-to-nitrogen dioxide ratio (HCHO/NO_2)—to determine regime thresholds. By correlating these variables and applying linear regression, the HCHO/NO_2 threshold for regime transition is identified as the point where WE-WD O_3 shifts from positive to negative values. The study includes an extensive trend analysis and trend reversal evaluation, ultimately establishing a global threshold of 3.5, with regional variations. This approach makes a valuable contribution to ozone mitigation strategies by providing a framework for more precise regime classification on a global scale. I suggest several revisions and clarifications before the paper can be considered for publication in Atmospheric Chemistry and Physics.

Reply: We would like to thank the reviewers for their time to review this paper. We have revised the manuscript following the reviewers' suggestions. Below are our point-by-point responses to the comments, along with the corresponding revisions.

Specific Comments:

1. *Given the nonlinear nature of O_3 formation due to complex VOC-NO_x interactions, comparing linear and nonlinear models would help justify the choice of linear regression for deriving regime threshold values.*

   Reply: We acknowledge that O_3 formation is nonlinearly dependent on NO_x and VOCs. The O_3 weekend effect captures this nonlinear dependence on NO_x, as it reflects the sensitivity of O_3 to changes in NO_x emissions on weekends, i.e., the derivative of O_3 with respect to NO_x. The transitioning point at which WE-WD = 0 is effectively at which $d[O_3]/d[NO_x] = 0$, which represent the transitioning point at which O_3 sensitivity to NO_x emission changes signs. Therefore, we think the linear regression method should be sufficient to capture the nonlinear O_3-NO_x-VOC chemistry.

   We also tested polynomial models of increasing complexity to examine the relationship between HCHO/NO_2 ratios and WE-WD O_3 differences. Our analysis shows that while higher-order polynomial models (up to cubic terms) do offer slightly improved statistical performance - as evidenced by reduced RMSE and increased R^2 values (see Figures 1-3 below) - these improvements are relatively modest in magnitude. More importantly, the nonlinear terms in these more complex models currently lack clear interpretation within the framework of O_3 formation regimes. After carefully weighing both the statistical and physicochemical considerations, we concluded that the original linear regression approach remains preferable. It provides sufficient fitting accuracy and straightforward physical interpretability, which consistent with the O_3 chemistry. We believe this balanced approach

ensures our threshold determination remains both statistically sound and chemically meaningful.

In the revised manuscript, we explain the reason why WE-WD can effectively capture the nonlinear O_3-NO_x-VOC chemistry as follows:

The WE-WD O_3 difference reflects the sensitivity of O_3 to emission reduction in NO_x on weekends, which is effectively the derivative of O_3 with respect to NO_x, and the transitioning point at which O_3 weekend effect crosses zero represents the transitioning point at which O_3 sensitivity to NO_x emission changes signs, which often corresponds to the peak O_3 production.

We derive threshold values for the $HCHO/NO_2$ ratio that delineate O_3 formation regimes by correlating the WE–WD differences in O_3 with $HCHO/NO_2$ using linear regression. The regime threshold corresponds to the intercept (zero-crossing point) of the regression line, where the sign of WE–WD O_3 changes.

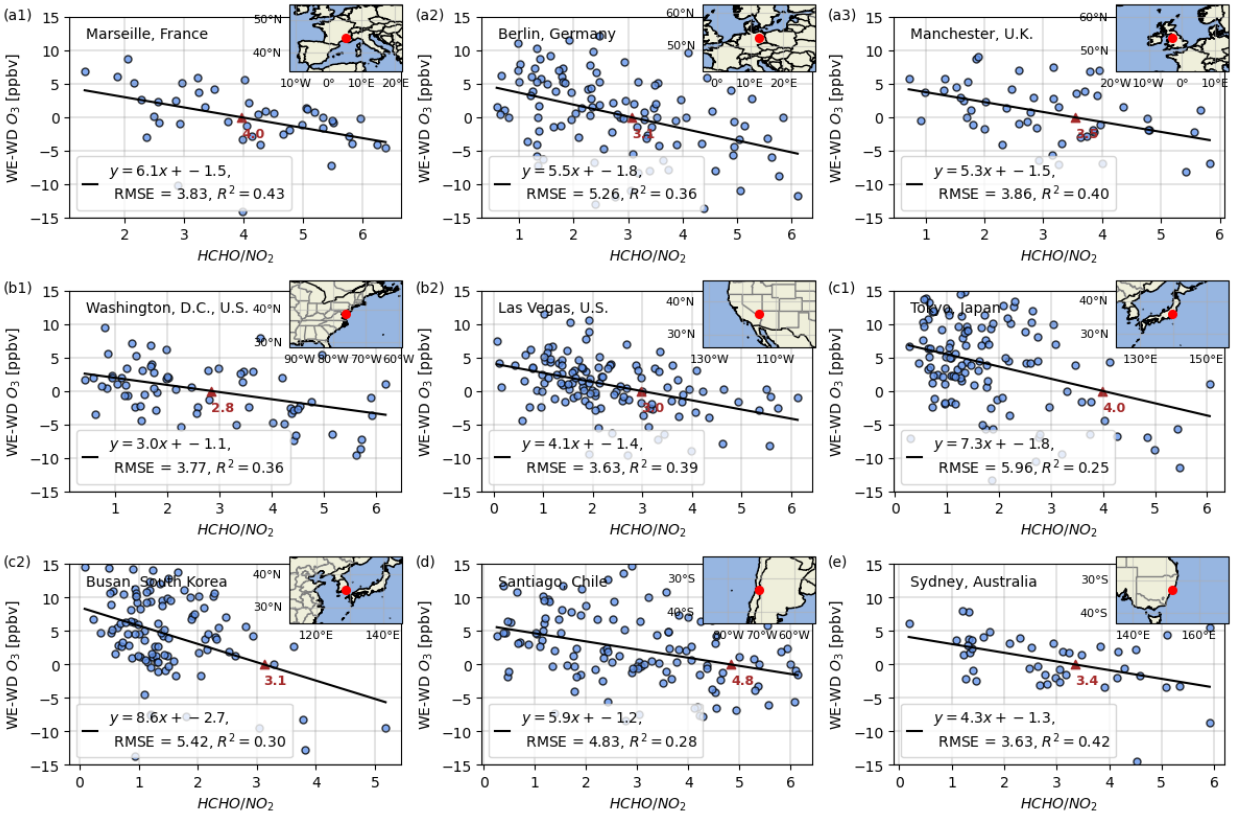

Figure 1: Scatter plot of the monthly average satellite-derived $HCHO/NO_2$ ratio versus the WE-WD O_3 concentration in 9 representative cities. The black line shows the fitted linear regression line with red triangles indicating inflection points where the regression line intersects the WE-WD O_3 = 0 baseline.

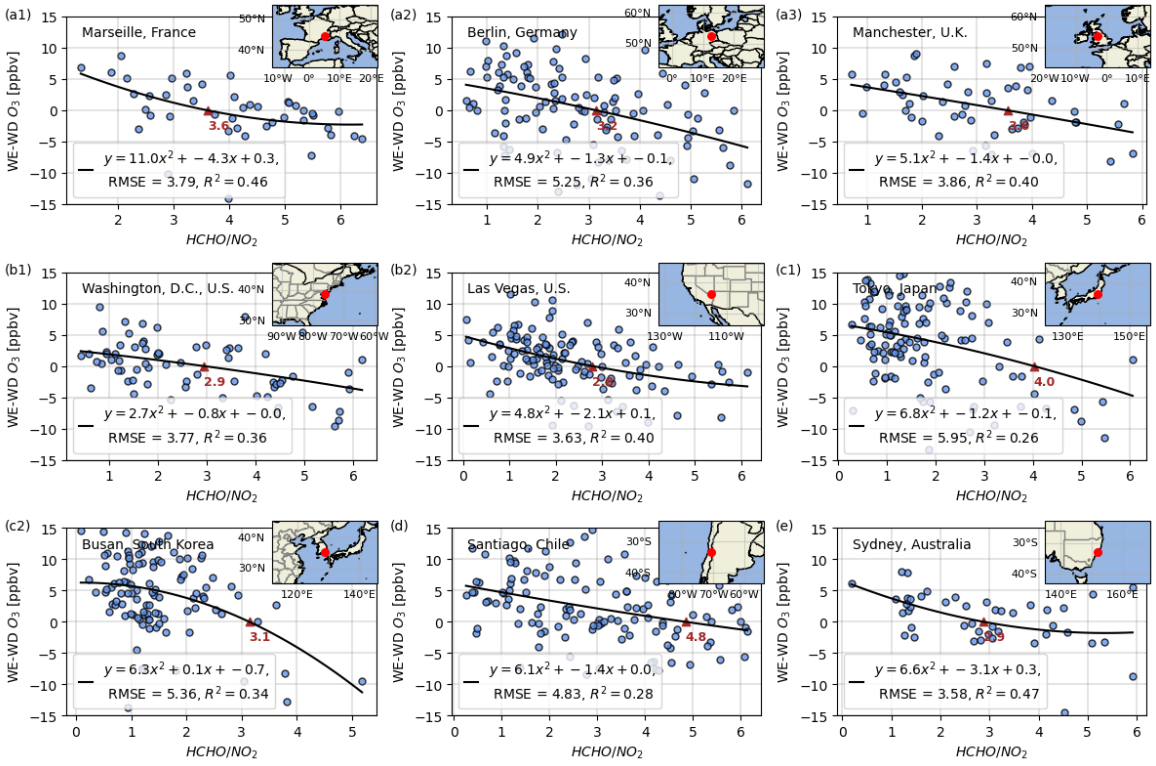

Figure 2: Second-order polynomial regression.

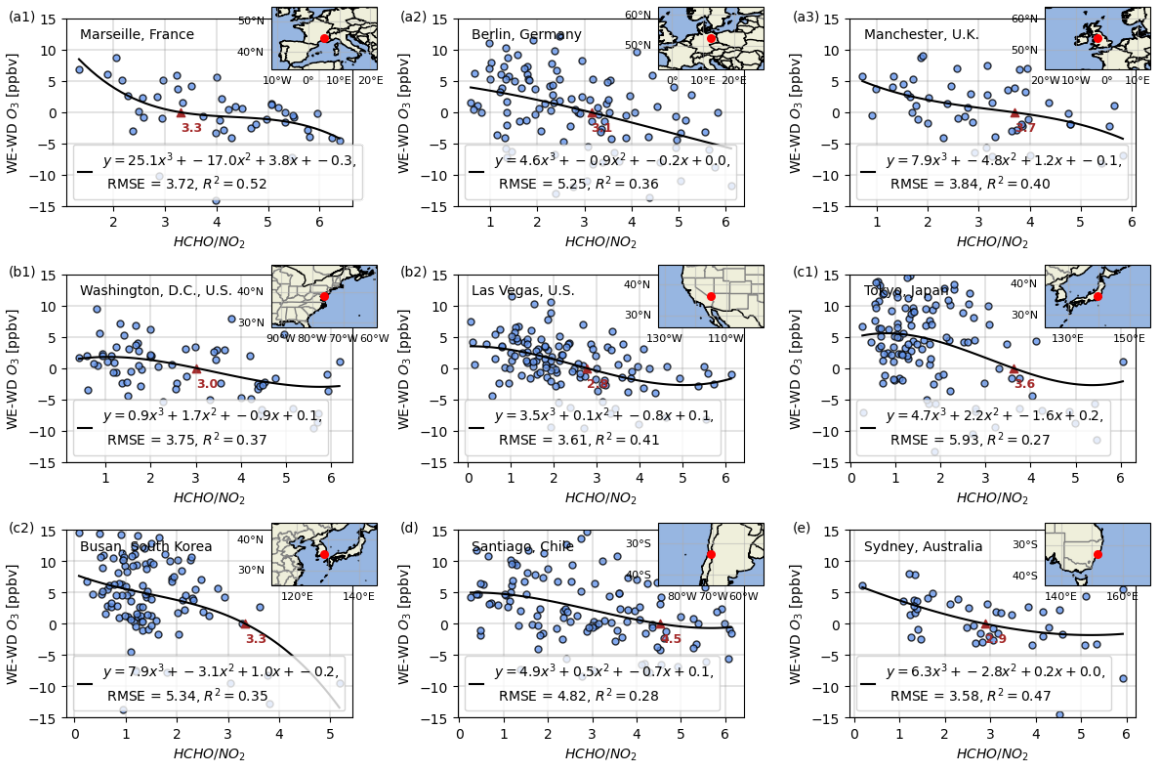

Figure 3: Third-order polynomial regression.

2. *A gradual transition between VOC-limited and NO_x-limited regimes is expected rather than an abrupt shift at a single point. Could nonlinear regression methods better capture this transition?*

Reply: We agree that the transition between VOC-limited and NO_x-limited regimes should be gradual rather than an abrupt shift. In our original manuscript, we employed a fixed threshold value primarily for simplification purposes, while recognizing this approach may not fully capture the transitional nature of regime shifts. The regime thresholds have uncertainties, and previous studies typically assume a range for regime threshold values (Jin et al., 2020; Jin et al., 2017; Sillman, 1999). To address this important point, we have improved our methodology in the revised manuscript:

1. Enhanced threshold characterization: When aggregating regional site data, we now not only identify the most frequent HCHO/NO_2 thresholds (peak HCHO/NO_2 frequencies, ($\tilde{\boldsymbol{x}}$)) but also determine the transitional range [$\boldsymbol{x_{lower}}$-$\boldsymbol{x_{upper}}$] based on the top 10% frequency interval to better quantify uncertainty, as illustrated in the new Figures 3b-c below.
2. For regional-scale analysis (Figure 9), we now employ region specific threshold ranges derived from Figure 3c. For grid-level assessment (Figure 10), we utilize regionally aggregated threshold ranges identified in Figure 3b, rather than using a global uniform value.

These improvements provide more accurate identification of O_3 regime transitions across different geographical contexts. We have accordingly updated all relevant discussions in Sections 3.3 and 3.4.

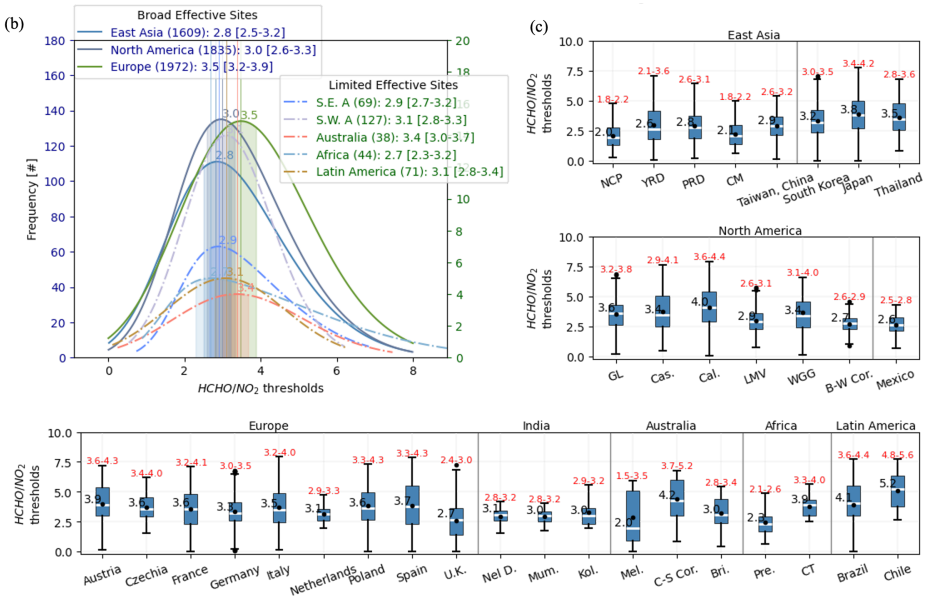

Figure 3: (b) Frequency distribution of HCHO/NO_2 thresholds across regions (R^2 > 0.2). Solid lines denote continents with >1500 valid sites; dashed lines represent regions with <150 sites. (c) Box plots of transition thresholds in economically advanced regions (marked in (a)). Black numbers: peak HCHO/NO_2 frequencies ($\tilde{\boldsymbol{x}}$); red range: top 10% frequency interval defining the transitional range [$\boldsymbol{x_{lower}}$, $\boldsymbol{x_{upper}}$].

3. *The long-term trend and trend reversal analyses rely on datasets with different spatial and temporal resolutions and measurement times. Although the datasets were harmonized, these differences may introduce biases in the observed trends and reversals. Were any considerations made to assess these biases?*

Reply: We have accounted for the differences in resolution and overpass time for the harmonization of satellite data products. Briefly, we use OMI as a reference to adjust GOME and SCIAMACHY columns as OMI has the finest spatial resolution and the overpass time of interest where captures the most active O_3 formation chemistry. For NO_2, the difference among satellite instruments is decomposed to two components: (1) differences caused by resolution; (2) difference due to overpass time. The difference caused by resolution is adjusted by comparing the differences in re-gridding Level-2 OMI NO_2 to fine-resolution (0.25° × 0.25°) grid versus a coarse-resolution (2° × 0.5°, resolution closer to that of GOME) grid. The difference in overpass time is derived from the mean difference between OMI and SCIAMACHY during overlapping years (2004 to 2012) at a coarse resolution (2° × 0.5°). For HCHO, as the spatial variations of HCHO are mostly regional, the harmonization only accounts for the difference caused by overpass time (Jin et al., 2020). We grid all Level-2 satellite HCHO products to 0.25° × 0.25°, and we adjust GOME and SCIAMACHY HCHO columns by adding the mean difference between SCIAMACHY and OMI during the overlapping period. We do not adjust for the difference between OMI and TROPOMI as their overpass time is close.

We have added detailed methodologies for the harmonization of the multi-satellite products in the revised manuscript:

To investigate the long-term changes in HCHO/NO_2, we construct annual average tropospheric NO_2 and HCHO VCD data from the GOME (1996-2001), SCIAMACHY (2002-2003) and OMI (2004-2020) and TROPOMI (2020 - 2022) datasets. GOME and SCIAMACHY and TROPOMI data are harmonized with reference to OMI data with a resolution of 0.25˚ × 0.25˚. The retrieval and harmonization scheme are described in Jin et al. (2020). Briefly, we use OMI as a reference to adjust GOME and SCIAMACHY columns as OMI has the finest spatial resolution and the overpass time of interest where captures the most active O_3 formation chemistry. For NO_2, the difference among satellite instruments is decomposed to two components: (1) difference due to resolution; (2) difference due to overpass time. The difference due to resolution is adjusted by comparing the differences in re-gridding Level-2 OMI NO_2 to fine-resolution (0.25° × 0.25°) grid versus a coarse-resolution (2° × 0.5°, resolution closer to that of GOME) grid. The difference in overpass time is derived from the mean difference between OMI and SCIAMACHY during overlapping years (2004 to 2012) at a coarse resolution (2° × 0.5°). For HCHO, as the spatial variations of HCHO are mostly regional, the harmonization only accounts for the difference

caused by overpass time (Jin et al., 2020). We grid all Level-2 satellite HCHO products to 0.25° × 0.25°, and adjust GOME and SCIAMACHY HCHO columns by adding the mean difference between SCIAMACHY and OMI during the overlapping period. We do not adjust for the difference between OMI and TROPOMI as their overpass time is close.

4. *The method used for trend and trend reversal evaluations assumes that trends are linear within 5-year windows and does not account for seasonality. Complementary statistical methods, such as seasonal-trend decomposition, could help verify the detected trends and reversals.*

Reply: Thanks for the reviewer's suggestion to address seasonality in our trend analysis. We used annual averages here for two reasons. First, satellite products (especially GOME and SCIAMACHY) at monthly scale have large uncertainties and noise, which would affect the derived trend. Second, while HCHO and NO_2 show seasonal variations, these cyclical patterns primarily manifest as short-term fluctuations that don't fundamentally alter the long-term decadal trends - similar to the NO_x trends shown in Georgoulias et al. (2019).
Our 5-year moving window approach was chosen to prioritize detection of persistent, policy-driven emission changes over sub-annual variability. This aligns with our study's focus on decadal-scale O_3 regime evolution rather than seasonal-scale variations.
We fully agree that seasonal-trend decomposition could provide valuable additional insights, particularly for identifying phase shifts (e.g., intensifying winter NO_x saturation in transitioning economies). While such analysis is beyond our current scope, we've added this as an important future research direction in the conclusion section:

Here, we examine the O_3 regime changes based on annual average $HCHO/NO_2$, but the O_3 chemical regime should vary seasonally (Jin et al., 2017; Jacob et al., 1995), typically becoming more NO_x-saturated in wintertime and more NO_x-limited in summertime. We exclude seasonal analysis because varying climatic definitions across regions would complicate cross-regional comparisons, and these cyclical variations do not substantially affect long-term decadal trends.

Conclusions: Here we focus on O_3 regime evolution annually, but O_3 regime also varies seasonally and diurnally. How the seasonal and diurnal variations of O_3 regime have evolved over time warrants further investigation. Further research could employ chemical-transport modeling to better understand both seasonal influences and the physical drivers of regional threshold differences, for instance, examining why economically developed regions characterized by higher values compared to less industrialized areas.

5. *Providing more details on the methodology for linking satellite and ground-based observations would improve clarity. Specifically, was the monthly WE-WD O_3 value calculated using all available hourly O_3 observations? Additionally, were all ground monitoring stations within a 0.25° grid included in computing the WE-WD O_3 averages before pairing with $HCHO/NO_2$ data?*

Reply: In the revised manuscript, we have added details in the description of the satellite-ground data linking method. Sundays were selected to represent weekends, and Tuesdays to Thursdays (mid-week days) to represent weekdays. The WE-WD O_3 analysis serves two parts of our study. One is in threshold determination (Figures 2-3): To establish robust relationships, we paired ground-based WE-WD O_3 data with the nearest grid HCHO/NO2 ratio data. The other is in regional trend analysis (Figures 7-8). Here, we included all ground stations within a region. This strategy balances precision (for threshold derivation) and representativeness (for regional trends), ensuring methodological rigor while addressing distinct analytical objectives. The methodology for linking WE-WD with satellite HCHO/NO_2 is added in the revised manuscript:

The WE-WD O_3 difference reflects the sensitivity of O_3 to emission reduction in NO_x on weekends, which is effectively the derivative of O_3 with respect to NO_x, and the transitioning point at which O_3 weekend effect crosses zero represents the transitioning point at which O_3 sensitivity to NO_x emission changes signs, which often corresponds to the peak O_3 production. In this study, WE-WD O_3 difference is quantified using a standardized protocol: **Sundays** is designated as weekends, while **Tuesdays–Thursdays** is designated weekdays, excluding Mondays and Fridays to minimize transitional effects from adjacent days. For each site and weekly interval throughout the observation period, we calculate the mean differences in WE-WD O_3. To calculate long-term trends of WE-WD O_3 in Section 3.3, all sites within the region are included. Given the global scope of this analysis and the inherent complexity in defining distinct O_3 seasons across various regions, we utilize all-year data without seasonal selection. Using *t*-test at each site to ascertain the statistical significance of WE-WD difference (p-value<0.05). Statistically significant WE-WD differences are identified at each site, and trends were evaluated using 5-year rolling intervals to dampen interannual meteorological variability (Pierce et al., 2010).

To build the relationship between observed O_3 weekend effect and satellite HCHO/NO_2 (Section 3.1), we mainly use OMI retrievals of HCHO and NO_2. OMI is selected as the primary satellite data source due to its unique combination of long-term continuity (2004-2020) and optimal afternoon overpass time. The early afternoon measurement period (13:00-14:00 local time) coincides with peak photochemical activity when O_3 production is most active, boundary layer heights are maximized, and solar zenith angles are minimized - all critical factors for obtaining high-quality retrievals of tropospheric HCHO and NO_2 columns (Jin et al., 2017; Jin and Holloway, 2015). We derive threshold values for the HCHO/NO_2 ratio that delineate O_3 formation regimes by correlating the WE–WD differences in O_3 with HCHO/NO_2 using linear regression. The regime threshold corresponds to the intercept (zero-crossing point) of the regression line, where the sign of WE–WD O_3 changes. To establish the relationship between HCHO/NO_2 ratios and WE-WD O_3, we extract the nearest gridded daily OMI data (0.125°×0.125°) corresponding to the ground-based O_3 monitoring stations. To ensure precise spatiotemporal matching, we pair the satellite overpass observations with surface measurements by averaging hourly O_3 concentrations at 13:00 and 14:00 local time (corresponding to OMI's overpass window).

6. *Although Figure 2 covers 2004–2022, some sites (e.g., Las Vegas, Los Angeles) have a higher number of data points. What explains these differences? Additionally, including the R^2 value would help assess the regression fit. Clarifying the criteria for selecting the nine representative urban areas would also be recommended.*

   Reply: The variation in data point counts across sites arises from differences in observational timelines and data availability within the TOAR-II database. For instance, the Manchester station (the U.K.) operated from 2006–2019 with intermittent gaps during 2007–2010, while Los Angeles (the U.S.) provided continuous measurements from 2004–2022, and Tokyo (Japan) spanned 2012–2021. These disparities are from station-specific factors such as maintenance schedules, data quality control exclusions, and monitoring network development. To ensure robustness, we used monthly averaged WE-WD O_3 values and excluded months with fewer than three weeks of valid data, minimizing noise from short-term fluctuations. This may also affect numbers of data points.
   The nine representative urban areas in Figure 2 were selected based on two criteria: long-term observational coverage (>10 years) and global representativeness. Sites in regions with sparse long-term data (e.g., South/Southeast Asia, Africa) or non-urban locations were excluded, as their limited records or atypical emission profiles could obscure regime transition signals.

   We have supplemented the reasons for such choices in the revised manuscript and included R^2 values in Figure 2 to quantify regression fit quality:

   To demonstrate our approach, we selected nine representative urban stations with long-term (>10 year) records, as shown in Error! Reference source not found.. These sites were chosen ensuring a balanced global representation while factoring in region site density (3 European, 2 North American, 2 Asian, 1 Australian, and 1 Latin American).

7. *Line 205. A discussion on the reasons behind the large spatial variability of threshold values would strengthen the analysis.*

   Reply: We have added discussions about the reasons behind the spatial variabilities of the threshold values as follows:

   The variations of the regime threshold values of $HCHO/NO_2$ are likely caused by several factors. First, here we use tropospheric column $HCHO/NO_2$ to represent the near-surface O_3 chemistry, which is affected by the relationships between column and surface HCHO and NO_2 (Jin et al., 2017). The column-to-surface relationship is determined by the boundary layer height and the vertical profiles of HCHO and NO_2, which should vary spatially (Adams et al., 2023; Zhang et al., 2016b). Second, HCHO is used as an indicator of VOCs, but the yield of HCHO from oxidation of VOCs varies with different species (Shen et al., 2019;

Chan Miller et al., 2016; Zhu et al., 2014). Regions dominated by biogenic VOC emissions like southeast U.S., tropical regions generally have larger HCHO yield (Wells et al., 2020; Palmer et al., 2007; Palmer et al., 2006). Third, the local chemical environmental may also differ spatially. For example, the lower thresholds in China are consistent with elevated regional NO_x levels (Jamali et al., 2020) and enhanced secondary aerosol formation in this region, which may promote radical loss (Li et al., 2019; Liu et al., 2012). Here we use statistical methods to derive the regime thresholds. Further attribution of the spatial variations is beyond the scope of this study, which warrant further investigation.

8. *Line 247. The methods indicate that trends were calculated using the Mann-Kendall test and Theil-Sen estimator, not linear regression.*

Reply: We thank the reviewer for catching this inconsistency. To clarify: our methodology employs two distinct trend analysis approaches tailored to the data characteristics. For ground-based WE-WD O_3 differences (TOAR data), we applied the Theil-Sen estimator with Mann-Kendall significance testing (Figure S5), as surface observations frequently contain localized anomalies (e.g. episodic pollution events) and data gaps across heterogeneous monitoring networks. This non-parametric approach ensures robustness against non-normal distributions and outliers. Conversely, for satellite-derived $HCHO/NO_2$ ratios, we applied linear regression (Figure 5), as these datasets undergo rigorous preprocessing (cloud filtering, spatial averaging, and anomaly correction) that minimizes outliers and satisfies normality assumptions required for parametric methods.
This differential approach aligns with established practices in atmospheric studies, where Theil-Sen is preferred for heterogeneous surface networks while linear regression remains valid for processed satellite products (Simon et al., 2024; Georgoulias et al., 2019). We have added more clear annotations in Figures 5 and S5 explicitly stating the trend analysis methods:

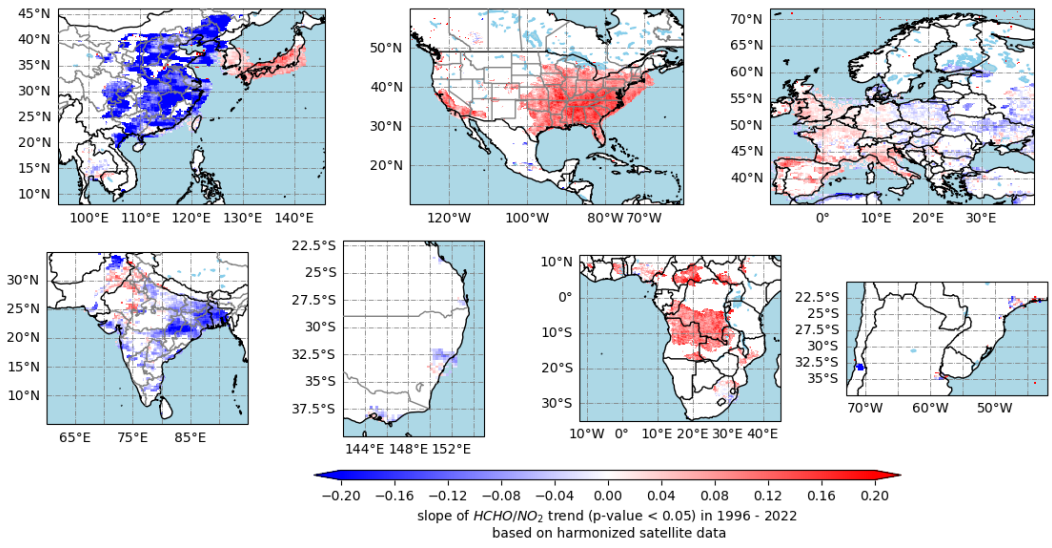

Figure 1: Satellite-based linear trends of tropospheric $HCHO/NO_2$ ratios (1996–2022) for grids with a mean NO_2 VCD > 1.5×10^{15} (molecules · cm^{-2}) and statistically significant trends at the 95 % confidence level.

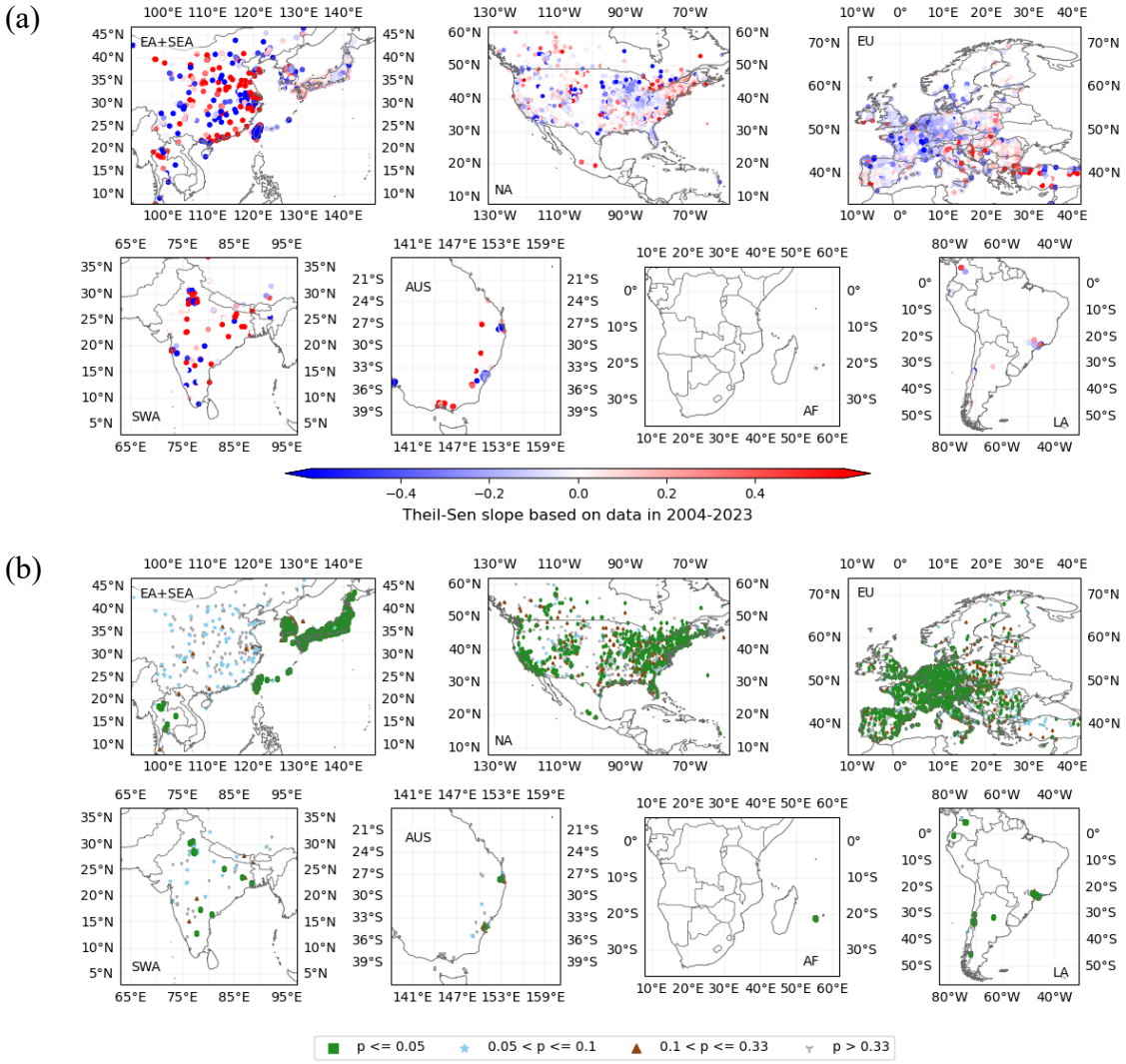

Figure S 1: (a) Map of WE-WD O_3 Theil–Sen slope (Raj and Koerts, 1992; Sen, 1968) and (b) p-value for the trend of timeseries using Mann– Kendall test (Kendall, 1975; Mann., 1945).

9. *Line 277. The decline in HCHO/NO_2 is attributed to NO_x reductions, but this interpretation appears counterintuitive.*

Reply: Thanks for catching this. We have corrected this in the revised manuscript as follows:

Post-2011, industrial VOC emissions rose by 20.46% from 2011-2017 (11,122.7 to 13,397.9 thousand tons/yr; Liu et al. (2021)), amplifying the post-2011 ratio recovery.

10. *Line 383. The identification of a single transition year for ozone sensitivity regimes seems somewhat ambiguous, given the temporal and spatial variability of regime classification thresholds, which may have also evolved over time. Focusing on trend changes rather than a specific transition year would provide a more robust interpretation.*

Reply: We fully acknowledge that regime classification thresholds may exhibit both temporal and spatial variability, making the determination of a single transition year potentially ambiguous. We consider this analysis valuable not only for determining transition years, but also for establishing a methodological approach to evaluated O_3 regime transitions. While previous studies have examined various aspects of O_3 regimes, our approach attempts to provide a more systematic quantification of these changes on a grid-level, particularly regarding transition timing and patterns. To address this, we have improved the methods in the revised manuscript by using region-specific transitional ranges defined by the top 10% frequency interval [$\boldsymbol{x_{lower}}$-$\boldsymbol{x_{upper}}$] (Figures 9-10 in the revised paper), and revised the relevant analysis focusing more on identifying trends of transit direction rather than precise years in the new Section 3.4.

Reference:

Adams, T. J., Geddes, J. A., and Lind, E. S.: New Insights Into the Role of Atmospheric Transport and Mixing on Column and Surface Concentrations of NO2 at a Coastal Urban Site, Journal of Geophysical Research: Atmospheres, 128, 10.1029/2022jd038237, 2023.

Chan Miller, C., Jacob, D. J., González Abad, G., and Chance, K.: Hotspot of glyoxal over the Pearl River delta seen from the OMI satellite instrument: implications for emissions of aromatic hydrocarbons, Atmospheric Chemistry and Physics, 16, 4631-4639, 10.5194/acp-16-4631-2016, 2016.

Georgoulias, A. K., van der A, R. J., Stammes, P., Boersma, K. F., and Eskes, H. J.: Trends and trend reversal detection in 2 decades of tropospheric NO2 satellite observations, Atmospheric Chemistry and Physics, 19, 6269-6294, 10.5194/acp-19-6269-2019, 2019.

Jacob, D. J., Horowitz, L. W., Munger, J. W., Heikes, B. G., Dickerson, R. R., Artz, R. S., and Keene, W. C.: Seasonal transition from NOx- to hydrocarbon-limited conditions for ozone production over the eastern United States in September, Journal of Geophysical Research, 100, 9315-9324, 10.1029/94jd03125, 1995.

Jamali, S., Klingmyr, D., and Tagesson, T.: Global-Scale Patterns and Trends in Tropospheric NO2 Concentrations, 2005–2018, Remote Sensing, 12, 10.3390/rs12213526, 2020.

Jin, X. and Holloway, T.: Spatial and temporal variability of ozone sensitivity over China observed from the Ozone Monitoring Instrument, Journal of Geophysical Research: Atmospheres, 120, 7229-7246, 10.1002/2015jd023250, 2015.

Jin, X., Fiore, A., Boersma, K. F., Smedt, I., and Valin, L.: Inferring changes in summertime surface ozone-NOx-VOC chemistry over U.S. urban areas from two decades of satellite and ground-based observations, Environmental Science & Technology, 54, 6518-6529, 10.1021/acs.est.9b07785, 2020.

Jin, X., Fiore, A. M., Murray, L. T., Valin, L. C., Lamsal, L. N., Duncan, B., Boersma, K. F., De Smedt, I., Abad, G. G., Chance, K., and Tonnesen, G. S.: Evaluating a space-based indicator of surface ozone-NOx-VOC sensitivity over midlatitude source regions and application to decadal trends, Journal of Geophysical Research: Atmospheres, 122, 10439-10488, 10.1002/2017JD026720, 2017.

Kendall, M. G.: Rank Correlation Methods, 4th edn., Charles Grif- fin, London1975.

Li, K., Jacob, D. J., Liao, H., Shen, L., Zhang, Q., and Bates, K. H.: Anthropogenic drivers of 2013-2017 trends in summer surface ozone in China, Proc Natl Acad Sci U S A, 116, 422-427, 10.1073/pnas.1812168116, 2019.

Liu, R., Zhong, M., Zhao, X., Lu, S., Tian, J., Li, Y., Hou, M., Liang, X., Huang, H., Fan, L., and

Ye, D.: Characteristics of industrial volatile organic compounds(VOCs) emission in China from 2011 to 2019, Environmental Science, 42, 5169-5179, 2021.
Liu, Z., Wang, Y., Gu, D., Zhao, C., Huey, L. G., Stickel, R., Liao, J., Shao, M., Zhu, T., Zeng, L., Amoroso, A., Costabile, F., Chang, C. C., and Liu, S. C.: Summertime photochemistry during CAREBeijing-2007: ROx budgets and O3 formation, Atmospheric Chemistry and Physics, 12, 7737-7752, 10.5194/acp-12-7737-2012, 2012.
Mann., H. B.: Nonparametric Tests Against Trend, Econometrica, 13, 245–259, 10.2307/1907187 1945.
Palmer, P. I., Barkley, M. P., Kurosu, T. P., Lewis, A. C., Saxton, J. E., Chance, K., and Gatti, L. V.: Interpreting satellite column observations of formaldehyde over tropical South America, Philos Trans A Math Phys Eng Sci, 365, 1741-1751, 10.1098/rsta.2007.2042, 2007.
Palmer, P. I., Abbot, D. S., Fu, T. M., Jacob, D. J., Chance, K., Kurosu, T. P., Guenther, A., Wiedinmyer, C., Stanton, J. C., Pilling, M. J., Pressley, S. N., Lamb, B., and Sumner, A. L.: Quantifying the seasonal and interannual variability of North American isoprene emissions using satellite observations of the formaldehyde column, Journal of Geophysical Research: Atmospheres, 111, 10.1029/2005jd006689, 2006.
Raj, B. and Koerts, J.: Henri Theil's Contributions to Economics and Econometrics, Advanced Studies in Theoretical and Applied Econometrics, Springer Dordrecht, 345–381 pp., 10.1007/978- 94-011-2546-8_20, 1992.
Sen, P. K.: Estimates of the Regression Coefficient Based on Kendall's Tau, Journal of the American Statistical Association, 63, 1379-1389, 10.1080/01621459.1968.10480934, 1968.
Shen, L., Jacob, D. J., Zhu, L., Zhang, Q., Zheng, B., Sulprizio, M. P., Li, K., De Smedt, I., González Abad, G., Cao, H., Fu, T. M., and Liao, H.: The 2005–2016 Trends of Formaldehyde Columns Over China Observed by Satellites: Increasing Anthropogenic Emissions of Volatile Organic Compounds and Decreasing Agricultural Fire Emissions, Geophysical Research Letters, 46, 4468-4475, 10.1029/2019gl082172, 2019.
Sillman, S.: The relation between ozone, NOx and hydrocarbons in urban and polluted rural environments, Atmospheric Environment, 33, 1821-1845, 10.1016/s1352-2310(98)00345-8, 1999.
Simon, H., Hogrefe, C., Whitehill, A., Foley, K. M., Liljegren, J., Possiel, N., Wells, B., Henderson, B. H., Valin, L. C., Tonnesen, G., Appel, K. W., and Koplitz, S.: Revisiting day-of-week ozone patterns in an era of evolving US air quality, Atmospheric Chemistry and Physics, 24, 1855-1871, 10.5194/acp-24-1855-2024, 2024.
Wells, K. C., Millet, D. B., Payne, V. H., Deventer, M. J., Bates, K. H., de Gouw, J. A., Graus, M., Warneke, C., Wisthaler, A., and Fuentes, J. D.: Satellite isoprene retrievals constrain emissions and atmospheric oxidation, Nature, 585, 225-233, 10.1038/s41586-020-2664-3, 2020.
Zhang, Y., Wang, Y., Chen, G., Smeltzer, C., Crawford, J., Olson, J., Szykman, J., Weinheimer, A. J., Knapp, D. J., Montzka, D. D., Wisthaler, A., Mikoviny, T., Fried, A., and Diskin, G.: Large vertical gradient of reactive nitrogen oxides in the boundary layer: Modeling analysis of DISCOVER-AQ 2011 observations, Journal of Geophysical Research: Atmospheres, 121, 1922-1934, 10.1002/2015jd024203, 2016.
Zhu, L., Jacob, D. J., Mickley, L. J., Marais, E. A., Cohan, D. S., Yoshida, Y., Duncan, B. N., González Abad, G., and Chance, K. V.: Anthropogenic emissions of highly reactive volatile organic compounds in eastern Texas inferred from oversampling of satellite (OMI) measurements of HCHO columns, Environmental Research Letters, 9, 10.1088/1748-9326/9/11/114004, 2014.